



# 1 To what extents do urbanization and air pollution affect fog?

2 Shuqi Yan<sup>1,2,3,4</sup>, Bin Zhu<sup>1,2,3,4,\*</sup>, Yong Huang<sup>5,6</sup>, Jun Zhu<sup>7</sup>, Hanqing Kang<sup>1,2,3,4</sup>, Chunsong Lu<sup>1,2,3,4</sup>, Tong Zhu<sup>8</sup>

3 <sup>1</sup>Collaborative Innovation Centre on Forecast and Evaluation of Meteorological Disasters, Nanjing University of Information  
4 Science & Technology, Nanjing, China

5 <sup>2</sup>Key Laboratory for Aerosol-Cloud-Precipitation of China Meteorological Administration, Nanjing University of Information  
6 Science & Technology, Nanjing, China

7 <sup>3</sup>Key Laboratory of Meteorological Disaster, Ministry of Education (KLME), Nanjing University of Information Science &  
8 Technology, Nanjing, China

9 <sup>4</sup>Special test field of National Integrated meteorological observation, Nanjing University of Information Science & Tech-  
10 nology, Nanjing, China

11 <sup>5</sup>Anhui Meteorology Institute, Key Lab of Atmospheric Science and Remote Sensing Anhui Province, Hefei 230031, China

12 <sup>6</sup>Shouxian National Climatology Observatory, Shouxian 232200, China

13 <sup>7</sup>Xiangshan Meteorological Bureau, Xiangshan 315700, China

14 <sup>8</sup>IMSG at NOAA/NESDIS/STAR, 5830 University Research Ct., College Park, MD 20740, USA

15

16 *Correspondence to:* Bin Zhu (binzhu@nuist.edu.cn)

17 **Abstract.** The remarkable development of China has resulted in rapid urbanization (urban heat island and dry island) and  
18 severe air pollution (aerosol pollution). Previous studies demonstrate that these two factors have either suppressing or pro-  
19 moting effects on fog, but what are the extents of their individual and combined effects? In this study, a dense radiation fog  
20 event in East China in January 2017 was reproduced by the WRF-Chem model, and the individual and combined effects of  
21 urbanization and aerosols on fog (indicated by liquid water content (LWC)) are quantitatively revealed. Results show that  
22 urbanization inhibits low-level fog, delays its formation and advances its dissipation due to higher temperatures and lower  
23 saturations. In contrast, upper-level fog could be enhanced because of the updraft-induced vapour convergence. Aerosols  
24 promote fog by increasing LWC, increasing droplet concentration and decreasing droplet effective radius. Further experi-  
25 ments show that the current pollution level in China is still below the critical aerosol concentration that suppresses fog. Ur-  
26 banization influences fog to a larger extent than do aerosols. When urbanization and aerosol pollution are combined, the  
27 much weaker aerosol promoting effect is counteracted by the stronger urbanization suppressing effect on fog. Budget analy-  
28 sis of LWC reveals that urban development (urbanization and aerosols) alters LWC profile and fog structure mainly by mod-  
29 ulating condensation/evaporation process. Our results infer that urban fog will be further reduced if urbanization keeps de-  
30 veloping and air quality keeps deteriorating in the future.



## 31 **1 Introduction**

32 During the past five decades, China has achieved remarkable developments, accompanied by strong anthropogenic activities  
33 (rapid urbanization and severe air pollution). Urbanization and air pollution have significantly affected climate change,  
34 monsoons, air quality, fog, clouds and precipitation (e.g., Li et al., 2016; Li et al., 2017). Many studies have linked the  
35 changes in clouds and precipitation to urbanization and aerosols. Urbanization destabilizes the boundary layer, which trig-  
36 gers strong updrafts and invigorates convection (e.g., Rozoff et al., 2003; Shepherd, 2005). Aerosols modify the macroscopic,  
37 microphysics, thermodynamics and radiative properties of clouds through complicated pathways, which are called as aero-  
38 sol-cloud-radiation interactions and have been systematically reviewed by Fan et al. (2016), Rosenfeld et al. (2014), Tao et al.  
39 (2012), etc. Fog can be viewed as a cloud (Leng et al., 2014) that occurs near the surface. Land use features and aerosol  
40 properties may instantly affect fog, so fog is more sensitive to anthropogenic activities than other types of clouds are (Zhu  
41 and Guo, 2016). Many studies have analysed the effects of urbanization and aerosols on fog, mostly in segregated manners.

42 Urbanization is featured with urban heat island (UHI) and dry island (UDI) effects. The urban surface has a lower albedo,  
43 which reduces the reflected solar radiation and enhances heat storage. Urban expansion decreases the coverage of cropland,  
44 water bodies and forestland, which reduces the sources of water vapour. As a result, urban areas commonly experience high-  
45 er temperatures and lower vapour contents. These conditions induce a lower supersaturation that is unfavourable for fog  
46 formation (Gu et al., 2019). In the long-term scale, urban fog days are reported to decrease significantly (e.g., Guo et al.,  
47 2016; LaDochy, 2005; Sachweh and Koepke, 1995; Shi et al., 2008; Yan et al., 2019). Although UHI and UDI inhibit  
48 near-surface fog, the upward motions can promote upper-level fog (Li et al., 2011; Niu et al., 2010b). Surface roughness and  
49 thermal circulation cause strong updrafts (Rozoff et al., 2003), which transfer water vapour aloft and cause wet island phe-  
50 nomenon in the upper-level (Kang et al., 2014). The fog at that altitude may be subsequently enhanced.

51 Aerosols exert sophisticated impacts on fog through direct (radiation) effects and indirect (microphysical) effects (Khain and  
52 Pinsky, 2018). Scattering aerosols block downwelling solar radiation in the daytime, thus delaying the dissipation and elon-  
53 gating the duration of fog (Shi et al., 2008; Maalick et al., 2016). Although they increase downwelling longwave radiation at  
54 night, scattering aerosols have negligible effects on the fog formation time (Stolaki et al., 2015; Maalick et al., 2016). The  
55 role of absorbing aerosols like BC on fog depends on its residence height. If BC resides above the fog layer, BC causes a  
56 dome effect (Ding et al., 2016) which blocks solar radiation and prevents the dissipation of fog (Bott, 1991). If BC resides  
57 within the fog layer, BC heats fog droplets and accelerates the dissipation of fog (Maalick et al., 2016). The aerosol indirect  
58 effect on cloud is addressed as one of the most uncertain factors in the IPCC report (IPCC, 2013). Aerosol concentration has  
59 a two-fold effect on fog, which is called as the boomerang pattern (Koren et al., 2008). Under saturation conditions, increas-  
60 ing aerosols commonly result in more CCNs. It promotes activation and condensation, yielding more but smaller droplets



61 and increasing cloud water content (Fan et al., 2018; Rosenfeld et al., 2008). These changes have two kinds of positive feed-  
62 back on fog (Maalick et al., 2016): more droplets cause stronger radiative cooling at fog top and enhance condensation (Jia et  
63 al., 2018); smaller droplet size inhibits sedimentation and the depletion of cloud water (Zhang et al., 2014). However, if aer-  
64 osol concentration exceeds a certain threshold, this promoting effect disappears (Quan et al., 2011) or even turns into a sup-  
65 pressing effect due to the strong vapour competition (Koren et al., 2008; Rangognio, 2009). Additionally, large-scale aerosol  
66 pollution can change weather patterns and affect large-scale fog formation conditions (Niu et al., 2010a). Ding et al. (2019)  
67 found that the dome effects of BC induce a land-sea thermal contrast and generate a cyclonic anomaly over coastal areas.  
68 This anomaly results in more vapor transported inland and strengthened advection-radiation fog.

69 Yan et al. (2019) analysed decadal trends of fog days and quantitatively proved that the inhibiting effects of urbanization  
70 outweigh the promoting effects of aerosols on fog during the mature urbanization stage. Their study inspires us to quantita-  
71 tively confirm the roles of urbanization and aerosols in a dense fog event by an online-coupled synoptic and air quality  
72 model, WRF-Chem. This event is a radiation fog event with weak synoptic forcing (detailed in Sect. 3.1), so the effects of  
73 urbanization and aerosols should be obvious. Determining the quantitative extents of urbanization effect, aerosol effect and  
74 their combined effect is an interesting topic, which has barely been studied previously to the best of our knowledge. This  
75 work facilitates the understanding of how anthropogenic activities affect the natural environment, fog (cloud) physics and  
76 aerosol-cloud interactions near the surface.

77 In this study, urbanization mainly refers to UHI and UDI associated with land use change and human activities, excluding the  
78 increasing aerosol pollution caused by urban expansion. Air pollution refers to aerosols and is indicated by anthropogenic  
79 emissions because aerosol concentration is highly proportional to emission intensity. Liquid water content (LWC) and  
80 cloud/fog droplet number concentration ( $N_d$ ) are two important parameters representing fog intensity and visibility. Follow-  
81 ing previous studies (e.g., Ding et al., 2019; Gu et al., 2019; Jia et al., 2018; Maalick et al., 2016; Yang et al., 2018), we use  
82 LWC as the indicator of fog to reveal different characteristics of fog in different experiments. This study is organized as fol-  
83 lows. The data, model and methods are described in Sect. 2. Section 3.1 overviews the fog event and provides preliminary  
84 evidence of how urban development affects fog. Section 3.2 evaluates the model performance. Sections 3.3 to 3.5 analyse the  
85 urbanization, aerosol and combined effects on fog. Section 3.6 discusses the rationality and reliability of the results.

## 86 **2 Data, model and methods**

### 87 **2.1 Data**

88 The first data are the hourly automatic weather station data from the Shouxian National Climate Observatory (SX; 32.4° N,



89 116.8° E, 23 m) that are used to evaluate the model performance. SX is a rural site surrounded by vast croplands and is ap-  
90 proximately 30 km away from the nearest large city (Fig. 1b). The data include horizontal visibility, temperature, relative  
91 humidity, wind direction and speed. The second data are the Himawari 8 satellite data that are used to represent fog area  
92 (<https://www.eorc.jaxa.jp/ptree/index.html>). Fog area is mainly indicated by the albedo at three visible bands: red (band 3,  
93 0.64  $\mu\text{m}$ ), green (band 2, 0.51  $\mu\text{m}$ ) and blue (band 1, 0.47  $\mu\text{m}$ ). The third data are the 3-hourly data from the Meteorological  
94 Information Comprehensive Analysis and Process System (MICAPS) (Li et al., 2010) that are also used to represent the fog  
95 area. The fourth data are the land use data from the Moderate Resolution Imaging Spectroradiometer Land Cover Type Ver-  
96 sion 6 data (MCD12Q1; <https://lpdaac.usgs.gov/products/mcd12q1v006>) in the year of 2017, the same as the simulation pe-  
97 riod. The data are resampled from 500 m to 30 arc-seconds (approximately 1 km) and replace the geological data of the WRF  
98 model.

## 99 2.2 Model configuration

100 The model used in this study is the WRF-Chem (V3.9.1.1) model. It is an online-coupled mesoscale synoptic and air quality  
101 model that considers the sophisticated interactions among various dynamic, physical and chemical processes (Chapman et al.,  
102 2009; Fast et al., 2006). WRF or WRF-Chem has been successfully used in simulating fog events (Jia and Guo, 2012; Jia and  
103 Guo, 2015; Jia et al., 2018) and exploring aerosol-cloud interactions (Fan et al., 2018). Two nest domains are set up (Fig. 1).  
104 The d01 domain has a size of 217 $\times$ 223 grids and a resolution of 6 km, covering the entire fog area of this event (Fig. 2a).  
105 The d02 domain has a size of 115 $\times$ 121 grids and a resolution of 2 km, covering SX and the adjacent areas. The land use data  
106 are replaced by MCD12Q1 data, which represent the latest condition.

107 Fog simulation is highly sensitive to vertical grids (Gultepe et al., 2007). A fine vertical resolution with a proper lowest  
108 model level can better resolve turbulences, thus yielding a reasonable fog structure (Yang et al., 2019). Here, 42 vertical lev-  
109 els are established with the first five  $\eta$  values of 1.000, 0.999, 0.998, 0.997, 0.996. There are 25 levels below the boundary  
110 layer (approximately 1500 m), and the lowest model level is approximately 8 m.

111 Fog simulation is also sensitive to physical schemes (Gu et al., 2019). Through numerous experiments, radiation, micro-  
112 physics and boundary schemes are found to significantly influence the model performance, and the boundary layer scheme  
113 plays a decisive role (Naira Chaouch et al., 2017). The radiation schemes are the RRTM longwave scheme and the Goddard  
114 shortwave scheme. The microphysical scheme is the Morrison double-moment scheme (Morrison et al., 2005). The boundary  
115 layer scheme is the YSU 1.5-order closure non-local scheme, which yields better results than do any other schemes. The  
116 major schemes are listed in Tab. 1.

117 The model is driven by the highest resolution product (0.125°, approximately 13 km) of ECMWF data



118 (<https://apps.ecmwf.int/datasets/data/interim-full-daily/levtype=sfc/>). The anthropogenic emissions are derived from the  
119 Multi-resolution Emission Inventory for China (MEIC) database (<http://www.meicmodel.org>). The simulation starts at  
120 2017-01-01 08:00 and ends at 2017-01-03 14:00, with the first 24 hours as the spin-up period (all the times here are in local  
121 time).

## 122 2.3 Sensitivity experiments

123 The study site is SX because only its visibility is observed hourly and is a multiple of 1 m, which is suitable for evaluating  
124 the model performance. To investigate the effects of urbanization and aerosols on fog, we change the land use and emission  
125 intensity around SX. Four experiments, i.e., u0e0, u3e0, u0e3 and u3e3 are designed. The u0e0 is the base experiment, with  
126 no urbanization and weak emission at SX. The u3e0 is set as the urbanization condition. The u0e3 is set as the polluted con-  
127 dition. The u3e3 is set as the urban development condition (urbanization and pollution coexist). The experiment settings are  
128 listed in Tab. 2.

129 On the setting of urbanized condition, we replace the land use of SX as that of Hefei, the most urbanized city and the capital  
130 of Anhui Province. The downtown of Hefei has a built area of approximately 570 km<sup>2</sup>. Therefore, the 11x13 box centered on  
131 SX (572 km<sup>2</sup>) is replaced by urban surface in the u3e0 and u3e3 experiments to represent the urbanization condition.

132 The downtown of Hefei has much higher emissions than SX. For example, the PM<sub>2.5</sub> emission rate of Hefei is 40 times  
133 higher than that of SX. To represent the polluted condition, the emission intensity of the aforementioned box is set to be  
134 equal to that of downtown Hefei in the u0e3 and u3e3 experiments.

## 135 2.4 Calculating visibility

136 The LWC is the proxy of fog as mentioned above. Since the LWC is not observed, and visibility (VIS) is related to LWC, the  
137 VIS is used to assess the model performance. VIS is not diagnosed by the model and can be parameterized by the function of  
138 LWC, N<sub>d</sub> or droplet effective radius (R<sub>e</sub>). Equation 1 (Kunkel, 1983) and 2 (Gultepe et al, 2006) are two parameterization  
139 methods.

$$\text{VIS}[\text{m}] = 27 \text{LWC}[\text{g cm}^{-3}]^{-0.88} \quad (1)$$

$$\text{VIS}[\text{m}] = 1002 (\text{LWC}[\text{g cm}^{-3}] \cdot \text{N}_d[\text{cm}^{-3}])^{-0.6473} \quad (2)$$

140 Another parameterization method is based on the Mie theory (Gultepe et al., 2017). VIS is inverse proportional to atmos-  
141 pheric extinction at visible wavelength. The extinction coefficient of cloud water ( $\beta_c$ ) is



$$\beta_c [\text{km}^{-1}] = \frac{3Q_{\text{ext}} \rho_a \text{LWC}}{4\rho_w R_e} \times 10^6 \quad (3)$$

142 where  $\rho_a$  ( $\rho_w$ ) is the air (water) density in  $\text{kg m}^{-3}$ , LWC is in  $\text{g kg}^{-1}$ ,  $R_e$  is in  $\mu\text{m}$ , and  $Q_{\text{ext}}$  is the extinction efficiency, which is  
143 assumed to be 2 for cloud droplets.

144 The atmospheric extinction ( $\beta$ ) is also largely contributed by aerosols ( $\beta_a$ ) and other types of hydrometeors. The model diag-  
145 noses  $\beta_a$  at 550 nm. No other types of hydrometeors occur in this fog case, so we assume  $\beta = \beta_a + \beta_c$ . Then VIS is determined  
146 by the Koschmieder rule (Koschmieder, 1924):  $\text{VIS}[\text{m}] = 3.912/\beta[\text{km}^{-1}] \times 1000$ .

147 During fog period (Fig. 4 shaded zone), the three methods nearly yield the same results (figure not shown), so the last meth-  
148 od is used to calculate the simulated VIS.

## 149 **3 Results and discussions**

### 150 **3.1 Overview of the fog event**

#### 151 **3.1.1 Formation condition and lifetime**

152 From 01 to 06 January 2017, East China is dominated by zonal circulation, with weak trough, ridge, pressure gradient and  
153 atmospheric diffusion (Zhang and Ma, 2017). Under this stable weather pattern, the accumulation of pollutants and water  
154 vapour promote the occurrence of fog-haze events. From the evening of 02 January to the noon of 03 January, a dense fog  
155 event occurs in wide regions of East China. The fog reaches its peak at 08:00 03 January, covering south Hebei, east Henan,  
156 west Shandong, Anhui, Jiangsu and Shanghai (Fig. 2a). Figure 4a shows the temporal variation of visibility at SX. The fog  
157 forms at 18:00 02 January and dissipates at 12:40 03 January. This is a radiation fog which is promoted by strong radiative  
158 cooling at night and weak easterly water vapour transport from northwest Pacific (Zhu et al., 2019).

#### 159 **3.1.2 Preliminary evidence of urban development affecting fog**

160 Lee (1987) and Sachweh and Koepke (1995) observed "fog holes" over urban areas on satellite images. Here, fog hole means  
161 the low liquid water path (LWP) region within the fog region, which is visualized as pixels with weak fog (high visibility) or  
162 clear sky surrounded by dense fog. These holes demonstrate that urban development (urbanization and aerosols) has a clear-  
163 ing effect on fog. In this fog event, fog holes are also present over urban areas on the Himawari 8 image at 11:00 03 January  
164 (Fig. 3). We assume that urbanization and air pollution could have profound effects on fog by reducing the LWP or advanc-



165 ing the dissipation of fog.

## 166 **3.2 Model evaluation and simulations**

167 The model performance is evaluated by comparing the fog spatial coverage. Satellite cloud image and modelled LWP can  
168 represent the observed and simulated fog zone, respectively (Jia et al., 2018). Figure 2 shows the Himawari 8 visible cloud  
169 image and the simulated LWP distribution at 08:00. The light white pixels and light red dots indicate the observed fog area.  
170 The model well captures the fog in south Hebei, east Henan, west Shandong, Anhui, Jiangsu and Shanghai.

171 The model performance is also evaluated by comparing the visibility and other basic parameters at the SX site (Fig. 4). Seen  
172 from the visibility, the simulated fog forms at 19:30, 1.5 h later than the observation, and dissipates at 12:20, 30 min earlier  
173 than the observation. During the fog period, the simulated visibility agrees well with the observation. The other parameters  
174 such as temperature, wind speed and relative humidity are also effectively reproduced by the model, with relative small  
175 RMSEs of 0.8 K, 0.7 m/s and 5.9 %, respectively. Overall, the model well captures the spatial feature and temporal evolution  
176 of the fog.

## 177 **3.3 Urbanization effects**

178 From different sensitivity experiments (u3e0, u0e3 and u3e3), we can deduce the extents of the separate or combined effects  
179 of urbanization and aerosols on fog. Figure 5 compares the LWC between u0e0 and u3e0. The general results are: (1) Before  
180 02:00, urbanization leads to a decreasing LWC in all layers. Fog forms on the surface at 22:30 in u3e0, 3 h later than in u0e0.  
181 (2) After 02:00, the LWC decreases in the low-level while it increases in the upper-level. Fog dissipates at 10:50 in u3e0, 1.5  
182 h earlier than in u0e0. To better explain the LWC difference, its profiles are shown in Fig. 6. At 23:00, although fog has  
183 formed in u3e0, the fog is rather weak compared with u0e0, which is caused by the higher temperature (Fig. 6f) and lower  
184 saturation associated with UHI and UDI. At 02:00, fog develops in u3e0, but its intensity (the value of LWC) cannot reach  
185 the same level as that in u0e0.

186 An interesting phenomenon is the opposite change of LWC in the low-level and upper-level after 02:00. This phenomenon  
187 can be explained by the role of updrafts. The increasing roughness length and extra warming in urban conditions could trig-  
188 ger horizontal wind convergence (Fig. S1) and the enhanced updrafts (Fig. 5c). The stronger updrafts in u3e0 affect conden-  
189 sation via two possible pathways: (1) the vertical transport of vapour ( $-w \frac{\partial q}{\partial z}$ ) and vertical convergence/divergence ( $-q \frac{\partial w}{\partial z}$ ) re-  
190 distribute water vapour and affect condensation; (2) the adiabatic cooling promotes condensation. The role of the first path-  
191 way is measured by vertical vapour flux divergence ( $\frac{1}{g} \frac{\partial(qw)}{\partial z}$ ). At 05:00, u3e0 shows a stronger vapour convergence above 110  
192 m (Fig. 6h), and the LWC increases above 130 m (Fig. 6c). At 08:00, u3e0 shows a stronger vapour convergence above 130



193 m (Fig. 6i), and the LWC increases above 170 m (Fig. 6d). Therefore, it is possible that the adiabatic cooling and up-  
194 draft-induced vapour flux convergence increase the vapour content and promote condensation in the upper-level, while the  
195 fog in the low-level is suppressed by the divergence of vapour flux. At 11:00, fog disappears at the ground in u3e0 likely due  
196 to the higher temperature (Fig. 6j). In summary, the UHI, UDI and updrafts alter the profile of LWC and reduce the LWP  
197 most of the time (Fig. 5c), and the decreasing LWP in the daytime can explain why fog holes occur above urban areas (Fig.  
198 3).

### 199 3.4 Aerosol effects

200 Figure 7 compares the LWC between u0e0 and u0e3. The formation time, dissipation time of fog and fog top show almost no  
201 changes. The LWC increases at almost all layers in the polluted condition. Accordingly, the LWP also increases (Fig. 7c). It  
202 is probable that the current pollution level of China always promotes fog occurrence. To testify whether the u0e3 is below  
203 the transition point of the boomerang pattern, eight additional experiments (D10, D7.5, D5, D2.5, M2.5, M5, M7.5 and M10)  
204 are performed. These experiments are the same as u0e3, except that the emissions around SX (the black box in Fig. 1b) are  
205 multiplied (the "M" prefix) or divided (the "D" prefix). For example, the name M2.5 means multiplying by 2.5 times; the  
206 name D10 means dividing by 10 times.

207 Figure 8 compares the LWC,  $N_d$ ,  $R_e$  and LWP among the nine emission-variant experiments. All the four parameters show  
208 the boomerang pattern, which demonstrates that the model is able to simulate the dual effects of aerosols. Below u0e3, the  
209 four parameters monotonically vary with emission level, indicating that aerosol pollution could always promote fog. This  
210 phenomenon is because stronger emissions produce more aerosols and CCN. Under saturation conditions, the larger amount  
211 of CCN boost activation and yield a higher  $N_d$ . The higher  $N_d$  reduces  $R_e$  and inhibits autoconversion and sedimentation  
212 (Twomey, 1977); thus, this situation decreases the depletion of fog water and increases the LWC. This promoting effect has  
213 been confirmed by many model studies (e.g., Maalick et al., 2016; Stolaki et al., 2015) and observations (e.g., Chen et al.,  
214 2012; Goren and Rosenfeld, 2012). The aerosol concentration of the transition point (experiment M2.5) is higher than that of  
215 u0e3 (Fig. 8), revealing that the current pollution level in China is still located in the promoting regime rather than the sup-  
216 pressing regime of fog occurrence, which is also found by Jia et al. (2018).

### 217 3.5 Combined effects of urbanization and aerosols

218 Figure 9 compares the LWC between u0e0 and u3e3. The u3e3-induced change is quite similar to but not the same as the  
219 u3e0-induced change. The time-height average of absolute change of LWC induced by u3e0, u0e3 and u3e3 are 0.120, 0.019,  
220 0.124 g kg<sup>-1</sup>, respectively. This result indicates that urbanization affects fog to a larger extent than do aerosols; when urbani-  
221 zation and aerosols are combined, the effect of aerosols is indiscernible. The LWP is also significantly suppressed in the day-



222 time, and the promoting effect of aerosols in Fig. 7c is indiscernible in Fig. 9c. To further explain the changes in LWC, we  
223 perform budget analysis of the LWC to determine which physical processes are the dominant contributors.

224 In WRF, the budget of LWC is composed of the following items,

$$\frac{\partial q_c}{\partial t} = - \underbrace{\left( u \frac{\partial}{\partial x} + v \frac{\partial}{\partial y} + w \frac{\partial}{\partial z} \right) q_c}_{\text{adv}} + \left( \frac{\partial q_c}{\partial t} \right)_{\text{PBL}} + \left( \frac{\partial q_c}{\partial t} \right)_{\text{micro}} + \left( \frac{\partial q_c}{\partial t} \right)_{\text{cumu}} \quad (4)$$

225 where  $q_c$  is LWC, and the subscripts denote advection, boundary layer, microphysical and cumulus processes, respectively.

226 The microphysical tendency is further decomposed into the following items,

$$\left( \frac{\partial q_c}{\partial t} \right)_{\text{micro}} = \left( \frac{\partial q_c}{\partial t} \right)_{\text{cold}} + \left( \frac{\partial q_c}{\partial t} \right)_{\text{auto}} + \left( \frac{\partial q_c}{\partial t} \right)_{\text{accr}} + \left( \frac{\partial q_c}{\partial t} \right)_{\text{sedi}} + \left( \frac{\partial q_c}{\partial t} \right)_{\text{cond/evap}} \quad (5)$$

227 where the subscripts denote cold phase processes, autoconversion, accretion, sedimentation and condensation/evaporation,  
228 respectively.

229 All the processes regarding precipitation and cold phase (the cumu, cold, auto and accr subscripts) are not analysed because  
230 no precipitation occurs, and the temperature is above 0°C in the simulated fog (figure not shown). The sum of microphysical  
231 (condensation/evaporation and sedimentation), boundary layer and advection tendencies is equal to the LWC distribution, so  
232 the contributions of other physical processes can be safely ignored.

233 We can also infer that to what extents the various physical processes affect fog through the sensitivity experiments (u3e0,  
234 u0e3 and u3e3). Additional aerosols weakly influence these processes (Fig. S2 right column) and subsequently result in weak  
235 LWC change (Fig. 7c). Compared with aerosols, urbanization effect is much more considerable (Fig. S3 right column); it  
236 dominantly accounts for the variation in physical tendencies from u0e0 to u3e3 (Fig. 10 right column). In u3e3 condition,  
237 urban development (urbanization and aerosols) induces different magnitude of changes in different physical tendencies. The  
238 relative magnitudes are 52.1, 38.3 and 9.6 % for the microphysical, boundary layer and advection processes, respectively,  
239 indicating that microphysics is most susceptible to urban development and contributes most to the LWC change. Among  
240 various microphysical processes, condensation/evaporation contributes most (72.7 %) to the change in microphysical ten-  
241 dency (Fig. 11 right column). The above results indicate that urban development affects the LWC mainly by modulating the  
242 condensation/evaporation process. Since u3e3 condition still witnesses higher temperatures and stronger updrafts (figure not  
243 shown), the notable variation in condensation/evaporation tendency induced by u3e3 can also be attributed to the predomi-  
244 nant role of UHI, UDI and updrafts. The mechanism has been analysed in Sect. 3.3.



### 245 **3.6 Discussions**

246 As mentioned above, urbanization influences fog to a larger extent than do aerosols; the LWC in fog does not vary substan-  
247 tially with pollution level. This section discusses the rationality and reliability of our results through mechanism analysis and  
248 observational evidence.

249 The sensitivity of cloud properties to aerosols depends on aerosol concentration and saturation environment. In convective  
250 clouds with intense upward motions and high saturations, the response of cloud properties to additional aerosols is signifi-  
251 cant ("aerosol-limited regime") (Fan et al., 2018). However, in fog with much weaker updrafts and lower saturations, this  
252 response could be more sensitive to vapour content rather than aerosol concentration ("vapour-limited regime"). It possibly  
253 implies that the LWC in fog varies slightly with pollution level but considerably with saturation condition that related to ur-  
254 banization. Our results reveal that the time-height average LWC varies within the extent of  $0.07\text{g kg}^{-1}$  when emission inten-  
255 sity varies within two orders of magnitude (Fig. 8). This relative weak response of the LWC to pollution level is also report-  
256 ed by Jia et al. (2018).

257 In terms of observational evidence, Yan et al. (2019) revealed that fog days in polluted regions of East China have decreased  
258 since the 1990s. Through quantitative analysis, the promoting effects of aerosols are weakening, while the suppressing ef-  
259 fects of urbanization are enhancing and dominantly cause this decrease. Sachweh and Koepke (1995) also claimed that the  
260 hindering effects of urbanization outweigh the promoting effects of aerosols on fog in southern Germany. Additionally, satel-  
261 lite images present discernible fog holes above urban areas (Fig. 3) (Lee, 1987; Sachweh and Koepke, 1995). Therefore,  
262 these observational evidence support the model results that the promoting effect of aerosols is counteracted by the hindering  
263 effect of urbanization. We believe that the results can also be applied to other cities in China because these cities commonly  
264 witness strong UHI, UDI and severe air pollution.

### 265 **4 Conclusions**

266 A dense radiation fog event occurred in East China from 02 to 03 January 2017. Satellite images show that fog holes occur  
267 over urban areas, demonstrating the remarkable effects of urbanization and air pollution on fog. Hence, the mechanism is  
268 investigated by the WRF-Chem model. The model well captures the spatial coverage and temporal evolution of the fog. Fur-  
269 thermore, the separate and combined effects of urbanization (refers to UHI and UDI) and air pollution (refers to aerosols) on  
270 fog (indicated by the LWC) are revealed, and the extents of these effects are quantitatively determined. Results show that:

271 Urbanization redistributes the LWC profile by the UHI, UDI effect and updrafts. The updrafts may be caused by surface



272 roughness and extra warming. The UHI and UDI suppress low-level fog, delay its formation by 3 h, and advance its dissipa-  
273 tion by 1.5 h. However, the upper-level fog could be enhanced due to the updraft-induced adiabatic cooling and vapour flux  
274 convergence. Urbanization reduces the LWP most of the time, and this reduction in the daytime can explain why fog holes  
275 are present above urban areas on satellite images.

276 Aerosols promote fog mainly by changing microphysical properties. The increasing emissions (aerosol concentration) pro-  
277 duce more CCN and fog droplets, which decreases  $R_c$  and inhibits sedimentation, thus leading to a higher LWC. Further sen-  
278 sitivity experiments show that the current pollution level in China is still below the transition point of the boomerang pattern  
279 that suppresses fog. The macroscopic properties such as fog top and lifetime remain nearly unchanged.

280 The role of urbanization far outweighs that of aerosols. Therefore, when they act together, the urbanization effect is domi-  
281 nant, and the aerosol effect is indiscernible. Budget analysis of LWC shows that increasing aerosols influence various physi-  
282 cal processes to a lesser extent, while urbanization influences these processes to a larger extent, eventually leading to a sub-  
283 stantial LWC change in urban development condition (urbanization and aerosols). In this condition, comparisons among  
284 various physical processes reveal that microphysics dominates the change in LWC, and condensation/evaporation dominates  
285 the change in microphysical tendency. This result highlights the importance of condensation/evaporation process in modu-  
286 lating the LWC profile and fog structure.

287 Mechanism analysis and the observational evidence support our key finding that urbanization influences fog to a much larger  
288 extent than do aerosol pollution. Therefore, we believe our results are reasonable and robust in radiation fog events without  
289 strong synoptic forcings, and the results can also be applied to other cities in China due to the similar urban development  
290 patterns. This study facilitates a better understanding of how anthropogenic activities affect the natural environment, fog  
291 (cloud) physics and aerosol-cloud interactions near the surface. We can also infer the future change of fog occurrence. Under  
292 the traditional urban development pattern, i.e., urbanization keeps developing and air quality keeps deteriorating, urban fog  
293 occurrence will be further reduced.

294

295 *Code and data availability.* Some of the data repositories have been listed in Sect. 2. The other data, model outputs and  
296 codes can be accessed by contacting Bin Zhu via [binzhu@nuist.edu.cn](mailto:binzhu@nuist.edu.cn).

297

298 *Author contributions.* SY performed the model simulation, data analysis and manuscript writing. BZ proposed the idea, su-  
299 pervised this work and revised the manuscript. YH provided the observation data at the SX site. JZ processed the observation  
300 data. HK offered helps to the model simulation. CL and TZ also contributed to the manuscript revision.



301

302 *Competing interests.* The authors declare that they have no conflict of interest.

303

304 *Acknowledgments.* We are grateful to the High Performance Computing Center of Nanjing University of Information Science  
305 and Technology for doing the numerical calculations in this work on its blade cluster system. We thank American Journal  
306 Experts (AJE) for the English language editing.

307

308 *Financial support.* This work is supported by the National Key Research and Development Program (2016YFA0602003)  
309 and the National Natural Science Foundation of China (91544229, 41575148, 41605091).

## 310 **References**

- 311 Abdul-Razzak, H. and Ghan, S. J.: A parameterization of aerosol activation 3. Sectional representation, *J. Geophys. Res.*, 107,  
312 AAC-1-AAC 1-6, <https://doi.org/10.1029/2001jd000483>, 2002.
- 313 Bott, A.: On the influence of the physico-chemical properties of aerosols on the life cycle of radiation fogs, *J. Aerosol. Sci.*, 21, 1–31,  
314 <https://doi.org/10.1007/BF00119960>, 1991.
- 315 Chapman, E. G., Gustafson, W. I., Easter, R. C., Barnard, J. C., Ghan, S. J., and Pekour, M. S.: Coupling aerosol-cloud-radiative processes  
316 in the WRF-Chem model: Investigating the radiative impact of elevated point sources, *Atmos. Chem. Phys.*, 9, 945–964,  
317 <https://doi.org/10.5194/acp-9-945-2009>, 2009.
- 318 Chen, Y. C., Christensen, M. W., Xue, L., Sorooshian, A., Stephens, G. L., Rasmussen, R. M., and Seinfeld, J. H.: Occurrence of lower  
319 cloud albedo in ship tracks, *Atmos. Chem. Phys.*, 12, 8223–8235, <https://doi.org/10.5194/acp-12-8223-2012>, 2012.
- 320 Di Vittorio, A. V. and Emery, W. J.: An automated, dynamic threshold cloud-masking algorithm for daytime AVHRR images over land,  
321 *IEEE Trans. Geosci. Remote Sensing*, 40, 1682–1694, <https://doi.org/10.1109/TGRS.2002.802455>, 2002.
- 322 Ding, A. J., Huang, X., Nie, W., Sun, J. N., Kerminen, V. - M., Petäjä, T., Su, H., Cheng, Y. F., Yang, X. - Q., Wang, M. H., Chi, X. G.,  
323 Wang, J. P., Virkkula, A., Guo, W. D., Yuan, J., Wang, S. Y., Zhang, R. J., Wu, Y. F., Song, Y., Zhu, T., Zilitinkevich, S., Kulmala, M.,  
324 and Fu, C. B.: Enhanced haze pollution by black carbon in megacities in China, *Geophys. Res. Lett.*, 43, 2873–2879,  
325 <https://doi.org/10.1002/2016gl067745>, 2016.
- 326 Ding, Q., Sun, J., Huang, X., Ding, A., Zou, J., Yang, X., and Fu, C.: Impacts of black carbon on the formation of advection–radiation fog  
327 during a haze pollution episode in eastern China, *Atmos. Chem. Phys.*, 19, 7759–7774, <https://doi.org/10.5194/acp-19-7759-2019>,  
328 2019.
- 329 Fan, J., Rosenfeld, D., Zhang, Y., Giangrande, S. E., Li, Z., and Machado, L. A. T.: Substantial convection and precipitation enhancements  
330 by ultrafine aerosol particles, *Science*, 359, 411–418, <https://doi.org/10.1126/science.aan8461>, 2018.
- 331 Fan, J., Wang, Y., Rosenfeld, D., and Liu, X.: Review of Aerosol–Cloud Interactions: Mechanisms, Significance, and Challenges, *J. Atmos.*  
332 *Sci.*, 73, 4221–4252, <https://doi.org/10.1175/JAS-D-16-0037.1>, 2016.
- 333 Fast, J. D., Gustafson, W. I., Easter, R. C., Zaveri, R. A., Barnard, J. C., Chapman, E. G., Grell, G. A., and Peckham, S. E.: Evolution of  
334 ozone, particulates, and aerosol direct radiative forcing in the vicinity of Houston using a fully coupled meteorology-  
335 chemistry-aerosol model, *J. Geophys. Res.*, 111, <https://doi.org/10.1029/2005jd006721>, 2006.



- 336 Goren, T. and Rosenfeld, D.: Satellite observations of ship emission induced transitions from broken to closed cell marine stratocumulus  
337 over large areas, *J. Geophys. Res.-Atmos.*, 117, -, <https://doi.org/10.1029/2012JD017981>, 2012.
- 338 Gu, Y., Kusaka, H., van Doan, Q., and Tan, J.: Impacts of urban expansion on fog types in Shanghai, China: Numerical experiments by  
339 WRF model, *Atmos. Res.*, 220, 57–74, <https://doi.org/10.1016/j.atmosres.2018.12.026>, 2019.
- 340 Gultepe, I., Tardif, R., Michaelides, S. C., Cermak, J., Bott, A., Bendix, J., Müller, M. D., Pagowski, M., Hansen, B., Ellrod, G., Jacobs, W.,  
341 Toth, G., and Cober, S. G.: Fog Research: A Review of Past Achievements and Future Perspectives, *Pure Appl. Geophys.*, 164, 1121–  
342 1159, <https://doi.org/10.1007/s00024-007-0211-x>, 2007.
- 343 Gultepe, I., Müller, M. D., and Boybeyi, Z.: A New Visibility Parameterization for Warm-Fog Applications in Numerical Weather Predic-  
344 tion Models, *J. Appl. Meteorol. Climatol.*, 45, 1469–1480, <https://doi.org/10.1175/jam2423.1>, 2006.
- 345 Gultepe, I., Milbrandt, J. A., and Zhou, B.: Marine fog: A review on microphysics and visibility prediction, in: Koračin D., Dorman C. (eds)  
346 Marine Fog: Challenges and Advancements in Observations, Modeling, and Forecasting, Springer, Cham, 50 pp., 2017.
- 347 Guo, T., Zhu, B., Kang, Z., Gui, H., and Kang, H.: Spatial and temporal distribution characteristic of fog days and haze days from  
348 1960~2012 and impact factors over the Yangtze River Delta Region, *China Environmental Science*, 36, 961 – 969,  
349 <https://doi.org/10.3969/j.issn.1000-6923.2016.04.001>, 2016. [in Chinese]
- 350 IPCC: Climate change 2013: The physical science basis, Contribution of Working Group I to the Fifth Assessment Report of the Intergov-  
351 ernmental Panel on Climate Change, Cambridge University Press, Cambridge, United Kingdom and New York, NY, USA, 1585 pp.,  
352 2013.
- 353 Jia, X. and Guo X.: Impacts of Anthropogenic Atmospheric Pollutant on Formation and Development of a Winter Heavy Fog Event, Chi-  
354 nese Journal of Atmospheric Sciences, 36, 995– 1008, <https://doi.org/10.3878/j.issn.1006-9895.2012.11200>, 2012. [in Chinese]
- 355 Jia, X. and Guo, X.: Impacts of Secondary Aerosols on a Persistent Fog Event in Northern China, *Atmospheric and Oceanic Science Let-  
356 ters*, 5, 401–407, <https://doi.org/10.1080/16742834.2012.11447022>, 2015.
- 357 Jia, X., Quan, J., Zheng, Z., Liu, X., Liu, Q., He, H., and Liu, Y.: Impacts of anthropogenic aerosols on fog in North China Plain, *J. Ge-  
358 ophys. Res.-Atmos.*, 124, 252–265, <https://doi.org/10.1029/2018jd029437>, 2018.
- 359 Kang, H., Zhu, B., Zhu, T., Sun, J., and Ou, J.: Impact of Megacity Shanghai on the Urban Heat-Island Effects over the Downstream City  
360 Kunshan, *Bound.-Layer Meteor.*, 152, 411–426, <https://doi.org/10.1007/s10546-014-9927-1>, 2014.
- 361 Khain, A. P. and Pinsky, M.: Modeling: A Powerful Tool for Cloud Investigation, in: Physical processes in clouds and cloud modeling,  
362 Cambridge University Press, Cambridge, United Kingdom and New York, NY, USA, 98 pp., 2018.
- 363 Koren, I., Martins, J. V., Remer, L. A., and Afargan, H.: Smoke invigoration versus inhibition of clouds over the Amazon, *Science*, 321,  
364 946–949, <https://doi.org/10.1126/science.1159185>, 2008.
- 365 Koschmieder, H.: Theorie der horizontalen sichtweite, *Beitr Phys.d.freien Atm*, 12, 171–181, 1924.
- 366 Kunkel, B. A.: Parameterization of Droplet Terminal Velocity and Extinction Coefficient in Fog Models, *J. Appl. Meteorol.*, 23, 34–41,  
367 [https://doi.org/10.1175/1520-0450\(1984\)023<0034:PODTVA>2.0.CO;2](https://doi.org/10.1175/1520-0450(1984)023<0034:PODTVA>2.0.CO;2), 1983
- 368 LaDochy, S.: The Disappearance of Dense Fog in Los Angeles: Another Urban Impact?, *Phys. Geogr.*, 26, 177–191,  
369 <https://doi.org/10.2747/0272-3646.26.3.177>, 2005.
- 370 Lee, T. F.: Urban clear islands in California central valley fog, *Mon. Weather Rev.*, 115, 1794–1796,  
371 [https://doi.org/10.1175/1520-0493\(1987\)1152.0.CO;2](https://doi.org/10.1175/1520-0493(1987)1152.0.CO;2), 1987.
- 372 Leng, C., Zhang, Q., Zhang, D., Xu, C., Cheng, T., Zhang, R., Tao, J., Chen, J., Zha, S., and Zhang, Y.: Variations of cloud condensation  
373 nuclei (CCN) and aerosol activity during fog-haze episode: a case study from Shanghai, *Atmos. Chem. Phys.*, 14, 12499–12512,  
374 <https://doi.org/10.5194/acp-14-12499-2014>, 2014.
- 375 Li, Y., Cao, L., Gao, S., and Luo, B.: The Current Stage and Development of MICAPS, *Meteorological Monthly*, 36, 50-55, 2010. [in Chi-  
376 nese]
- 377 Li, Z., Guo, J., Ding, A., Liao, H., Liu, J., Sun, Y., Wang, T., Xue, H., Zhang, H., and Zhu, B.: Aerosol and boundary-layer interactions and  
378 impact on air quality, *Natl. Sci. Rev.*, 4, 810–833, <https://doi.org/10.1093/nsr/nwx117>, 2017.



- 379 Li, Z., Lau, W. K. M., Ramanathan, V., Wu, G., Ding, Y., Manoj, M. G., Liu, J., Qian, Y., Li, J., Zhou, T., Fan, J., Rosenfeld, D., Ming, Y.,  
380 Wang, Y., Huang, J., Wang, B., Xu, X., Lee, S. S., Cribb, M., Zhang, F., Yang, X., Zhao, C., Takemura, T., Wang, K., Xia, X., Yin, Y.,  
381 Zhang, H., Guo, J., Zhai, P. M., Sugimoto, N., Babu, S. S., and Brasseur, G. P.: Aerosol and monsoon climate interactions over Asia,  
382 *Rev. Geophys.*, 54, 866–929, <https://doi.org/10.1002/2015RG000500>, 2016.
- 383 Li, Z., Yang, J., Shi, C., and Pu, M.: Urbanization Effects on Fog in China: Field Research and Modeling, *Pure Appl. Geophys.*, 169, 927–  
384 939, <https://doi.org/10.1007/s00024-011-0356-5>, 2011.
- 385 Maalick, Z., Kühn, T., Korhonen, H., Kokkola, H., Laaksonen, A., and Romakkaniemi, S.: Effect of aerosol concentration and absorbing  
386 aerosol on the radiation fog life cycle, *Atmos. Environ.*, 133, 26–33, <https://doi.org/10.1016/j.atmosenv.2016.03.018>, 2016.
- 387 Morrison, H., Curry, J. A., and Khvorostyanov, V. I.: A new double-moment microphysics parameterization for application in cloud and  
388 climate models. Part I: Description, *J. Atmos. Sci.*, 62, 1665–1677, <https://doi.org/10.1175/JAS3446.1>, 2005.
- 389 Naira Chaouch, Marouane Temimi, Michael Weston, and Hosni Ghedira: Sensitivity of the meteorological model WRF-ARW to planetary  
390 boundary layer schemes during fog conditions in a coastal arid region, *Atmos. Res.*, 187, 106–127,  
391 <https://doi.org/10.1016/j.atmosres.2016.12.009>, available at: <http://www.sciencedirect.com/science/article/pii/S0169809516307116>,  
392 2017.
- 393 Niu, F., Li, Z., Li, C., Lee, K., and Wang, M.: Increase of wintertime fog in China: Potential impacts of weakening of the Eastern Asian  
394 monsoon circulation and increasing aerosol loading, *J. Geophys. Res.*, 115, <https://doi.org/10.1029/2009jd013484>, 2010a.
- 395 Niu, S., Lu, C., Yu, H., Zhao, L., and Lü, J.: Fog research in China: An overview, *Adv. Atmos. Sci.*, 27, 639–662,  
396 <https://doi.org/10.1007/s00376-009-8174-8>, 2010b.
- 397 Rangognio, J.: Influence of aerosols on the formation and development of radiation fog, *Atmos. Chem. Phys.*, 9, 17963–18019,  
398 <https://doi.org/10.5194/acpd-9-17963-2009>, 2009.
- 399 Rosenfeld, D., Meinrat O. Andreae, Asmi, A., Chin, M., and Johannes Quaas: Global observations of aerosol-cloud-precipitation-climate  
400 interactions, *Rev. Geophys.*, 52, 750–808, <https://doi.org/10.1002/2013RG000441>, 2014.
- 401 Rosenfeld, D., Lohmann, U., Raga, G. B., O'Dowd, C. D., Kulmala, M., Fuzzi, S., Reissell, A., and Andreae, M. O.: Flood or drought:  
402 how do aerosols affect precipitation?, *Science*, 321, 1309–1313, <https://doi.org/10.1126/science.1160606>, 2008.
- 403 Rozoff, C. M., Cotton, W. R., and Adegoke, J. O.: Simulation of St. Louis, Missouri, Land Use Impacts on Thunderstorms, *J. Appl. Mete-*  
404 *orol.*, 42, 716–738, [https://doi.org/10.1175/1520-0450\(2003\)042<0716:SOSLML>2.0.CO;2](https://doi.org/10.1175/1520-0450(2003)042<0716:SOSLML>2.0.CO;2), 2003.
- 405 Sachweh, M. and Koepke, P.: Radiation fog and urban climate, *Geophys. Res. Lett.*, 22, 1073–1076, <https://doi.org/10.1029/95gl00907>,  
406 1995.
- 407 Shepherd, J. M.: A Review of Current Investigations of Urban-Induced Rainfall and Recommendations for the Future, *Earth Interact.*, 9,  
408 1–27, <https://doi.org/10.1175/ei156.1>, 2005.
- 409 Shi, C., Roth, M., Zhang, H., and Li, Z.: Impacts of urbanization on long-term fog variation in Anhui Province, China, *Atmos. Environ.*, 42,  
410 8484–8492, <https://doi.org/10.1016/j.atmosenv.2008.08.002>, 2008.
- 411 Stolaki, S., Haefelin, M., Lac, C., Dupont, J. C., Elias, T., and Masson, V.: Influence of aerosols on the life cycle of a radiation fog event.  
412 A numerical and observational study, *Atmos. Res.*, 151, 146–161, <https://doi.org/10.1016/j.atmosres.2014.04.013>, 2015.
- 413 Tao, W. K., Chen, J. P., Li, Z., Wang, C., and Zhang, C.: Impact of aerosols on convective clouds and precipitation, *Rev. Geophys.*, 50,  
414 6837, <https://doi.org/10.1029/2011RG000369>, 2012.
- 415 Twomey, S. A.: The Influence of Pollution on the Shortwave Albedo of Clouds, *J. Atmos. Sci.*, 34, 1149–1154,  
416 [https://doi.org/10.1175/1520-0469\(1977\)034<1149:tiopot>2.0.co;2](https://doi.org/10.1175/1520-0469(1977)034<1149:tiopot>2.0.co;2), 1977.
- 417 Yan, S., Zhu, B., and Kang, H.: Long-term fog variation and its impact factors over polluted regions of East China, *J. Geophys.*  
418 *Res.-Atmos.*, 124, 1741–1754, <https://doi.org/10.1029/2018JD029389>, 2019.
- 419 Yang, Y., Hu, X., Gao, S., and Wang, Y.: Sensitivity of WRF simulations with the YSU PBL scheme to the lowest model level height for a  
420 sea fog event over the Yellow Sea, *Atmos. Res.*, 215, 253–267, <https://doi.org/10.1016/j.atmosres.2018.09.004>, 2019.
- 421 Zhang, N. and Ma, X.: Analysis of the June 2018 Atmospheric Circulation and Weather, *Meteorological Monthly*, 43, 508–512,  
422 <https://doi.org/10.7519/j.issn.1000-0526.2017.04.014>, 2017. [in Chinese]



- 423 Zhang, X., Musson-Genon, L., Dupont, E., Milliez, M., and Carissimo, B.: On the Influence of a Simple Microphysics Parametrization on  
424 Radiation Fog Modelling: A Case Study During ParisFog, *Bound.-Layer Meteor.*, 151, 293–315,  
425 <https://doi.org/10.1007/s10546-013-9894-y>, 2014.
- 426 Zhu, B. and Guo, T.: Review of the Impact of Air Pollution on Fog, *Advances in Meteorological Science and Technology*, 6, 56– 63,  
427 <https://doi.org/10.3969/j.issn.2095-1973.2016.02.006>, 2016. [in Chinese]
- 428 Zhu, J., Zhu, B., Huang, Y., An, J., and Xu, J.: PM<sub>2.5</sub> vertical variation during a fog episode in a rural area of the Yangtze River Delta,  
429 China, *Sci. Total. Environ.*, 685, 555–563, <https://doi.org/10.1016/j.scitotenv.2019.05.319>, 2019.
- 430



431 Table 1. Summary of major parameterization schemes.

Scheme	Option
Boundary layer	YSU
Longwave radiation	RRTM
Shortwave radiation	New Goddard
Microphysics	Morrison
Surface layer	MM5 similarity
Land surface	Noah
Urban surface	Urban canopy model
Gas phase chemistry	CBMZ
Aerosol chemistry	MOSAIC (4-bin)
Aerosol-cloud-radiation interactions	All turned on
Aerosol activation	Abdul-Razzak and Ghan (2002)

432

433



434 Table 2. Settings of sensitive experiments. "N" represents no changes.

Case name	Description	Underlying surface	Anthropogenic emission
u0e0	base condition	N	N
u3e0	urbanization condition	the 11x13 grid centered on SX is replaced by urban surface	N
u0e3	polluted condition	N	the 11x13 grid centered on SX is replaced by the emission of Hefei downtown
u3e3	urbanization and polluted condition	same as u3e0	same as u0e3

Effect	Description
u3e0-u0e0	urbanization effect
u0e3-u0e0	aerosol effect
u3e3-u0e0	urbanization and aerosol effect

435

436

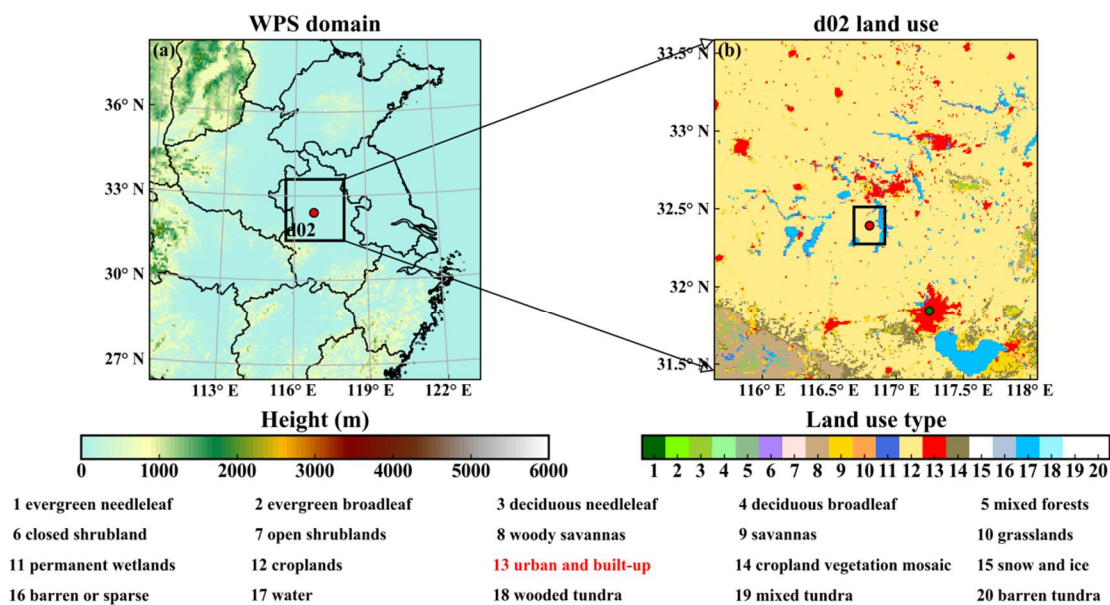
437

438

439



440



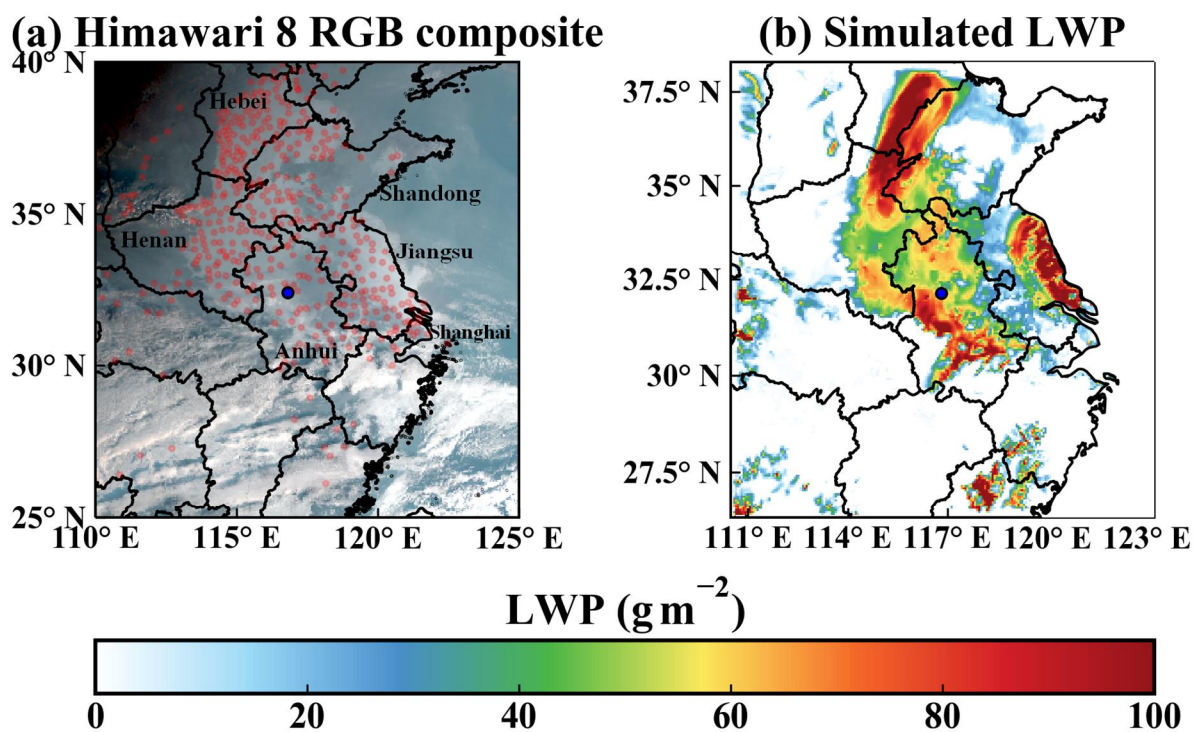
441

442 Figure 1. (a) The WRF domain overlaid with terrain height. (b) The land use distribution of domain d02. The green dot  
443 is Hefei, the capital of Anhui Province. The two red dots are the SX site. The land use and emissions of the 22 km × 26  
444 km black box in the center of (b) will be altered in the sensitivity experiments.

445



446

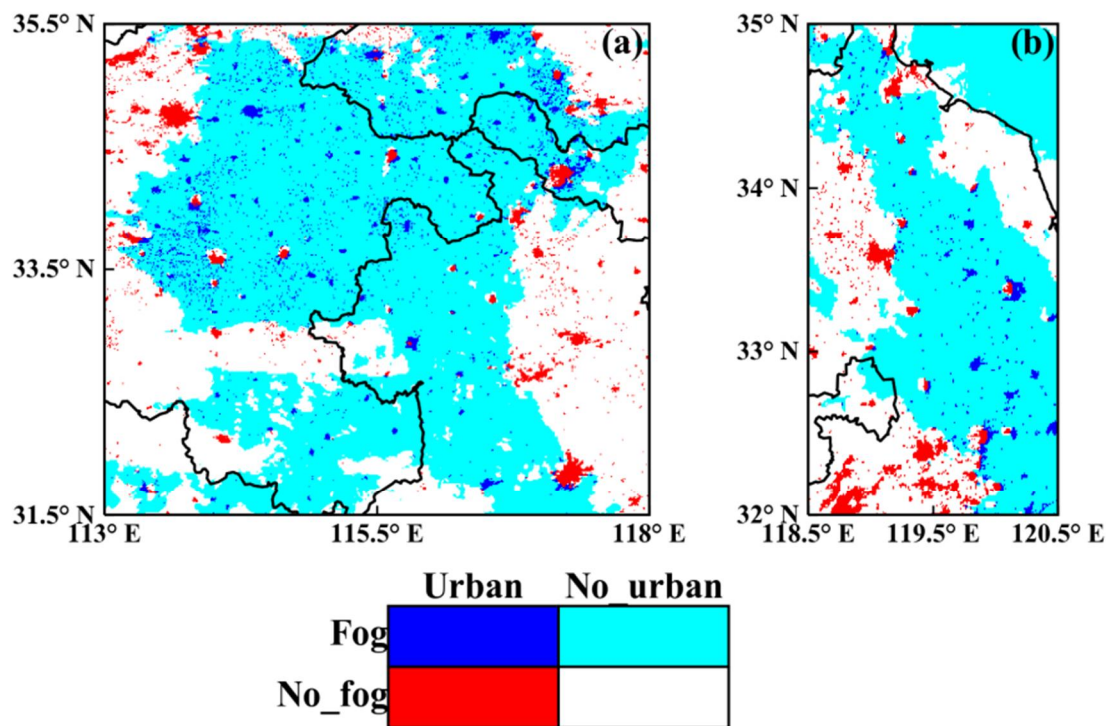


447

448 Figure 2. The performance of the simulated fog zone at 08:00 03 January. (a) Himawari 8 RGB composite cloud image  
449 overlaid with the MICAPS observation sites (light red dots) at which fog was observed (relative humidity > 90 % and  
450 VIS < 1 km). (b) Simulated LWP distribution. Only LWC below 1500 m are integrated. The blue dots are the SX site.  
451



452



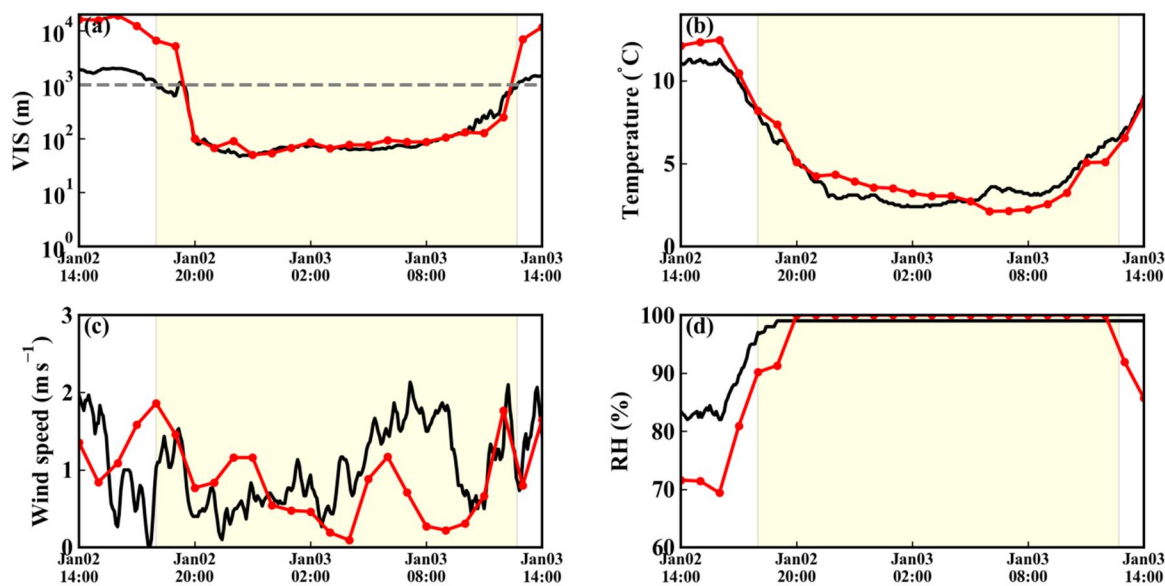
453

454 Figure 3. Two sub-regions (a and b) with obvious fog holes on the Himawari 8 image at 11:00 03 January. The fog  
455 zone, which is represented by albedo  $> 0.45$  (at  $0.64 \mu\text{m}$ ) and brightness temperature  $> 266 \text{ K}$  (at  $12.4 \mu\text{m}$ ) (Di Vittorio  
456 et al., 2002), is marked with cold colours (blue or cyan). The urban areas are marked with blue or red. The red and  
457 white pixels surrounded or semi-surrounded by cold colours are fog holes, and among these pixels, the red pixels indi-  
458 cate the fog holes over urban areas.

459



460

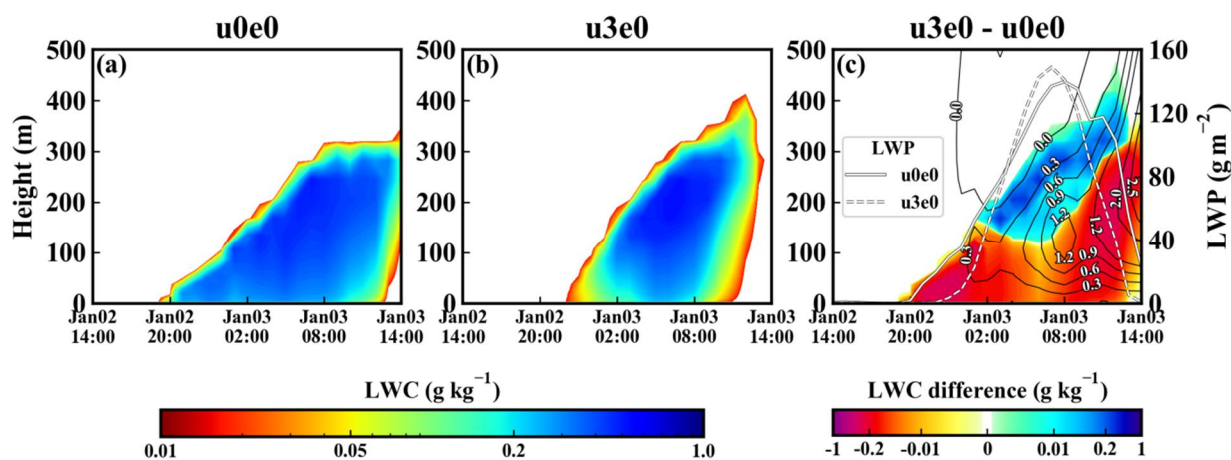


461

462 Figure 4. The performance of the simulated meteorological parameters at the SX site. (a) VIS. (b) air temperature. (c)  
463 10-minute average wind speed. (d) Relative humidity (RH). The red dotted lines represent the model results, and the  
464 black lines are the observations. The fog period (VIS < 1 km and RH > 90 %) is shaded with light yellow.  
465

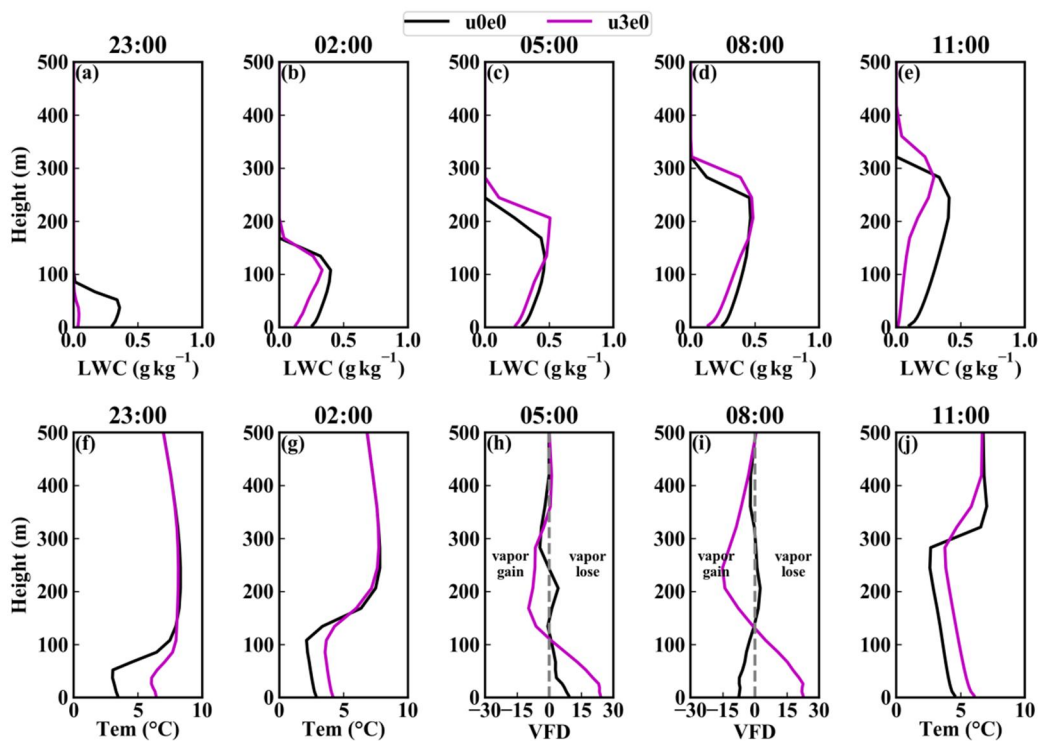


466





472



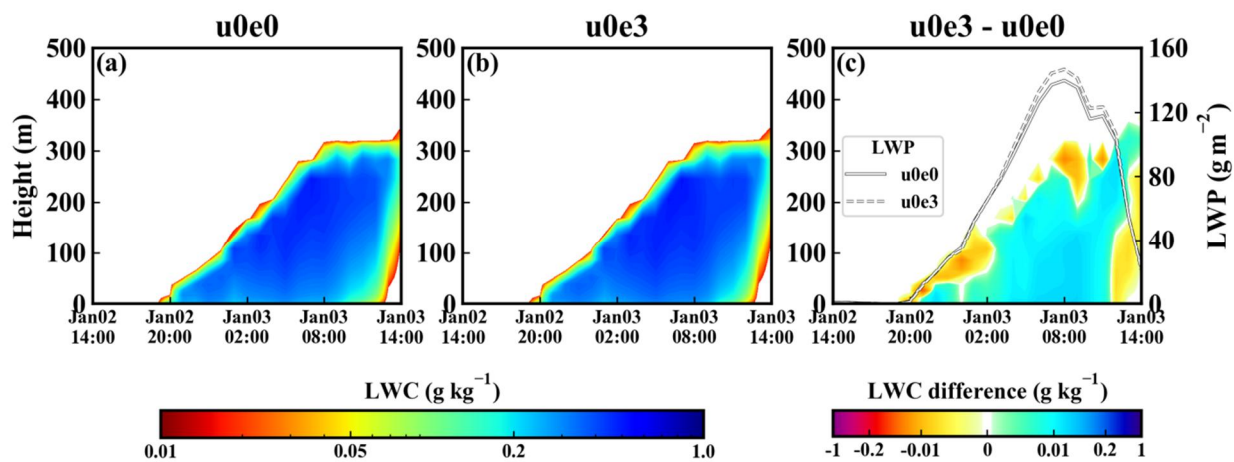
473

474 Figure 6. Profiles of the LWC (first row), temperature (Tem) (f, g, j) and vertical vapour flux divergence (VFD) (h, i)  
475 ( $\text{g h}^{-1} \text{m}^{-2} \cdot \text{hpa}^{-1}$ ) in u0e0 and u3e0 at different times.

476



477



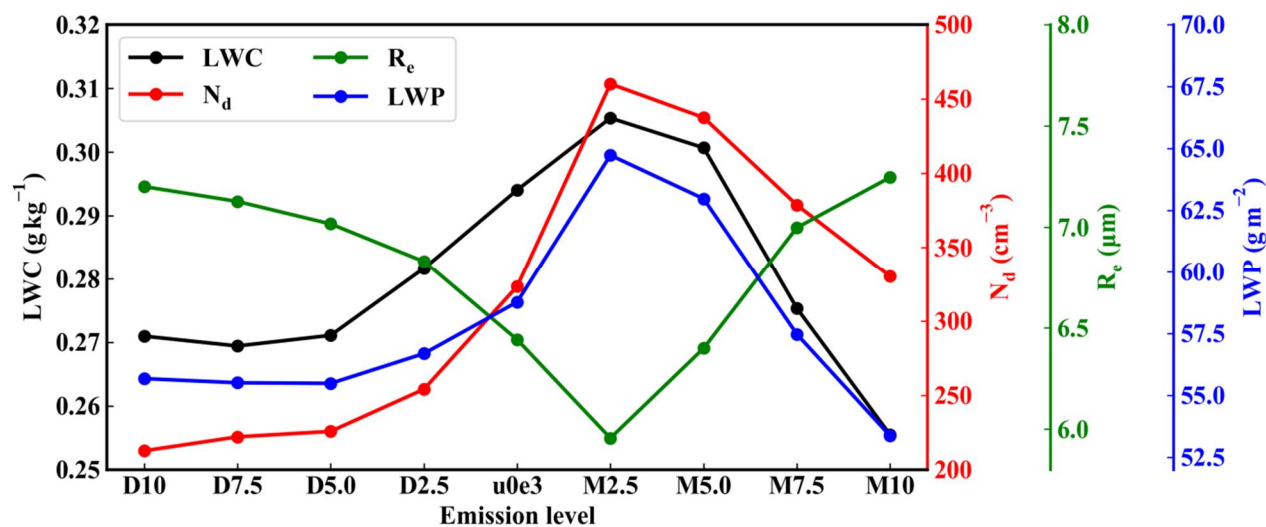
478

479 Figure 7. Similar to Fig. 5, but for the aerosol effect (u0e3 minus u0e0).

480



481



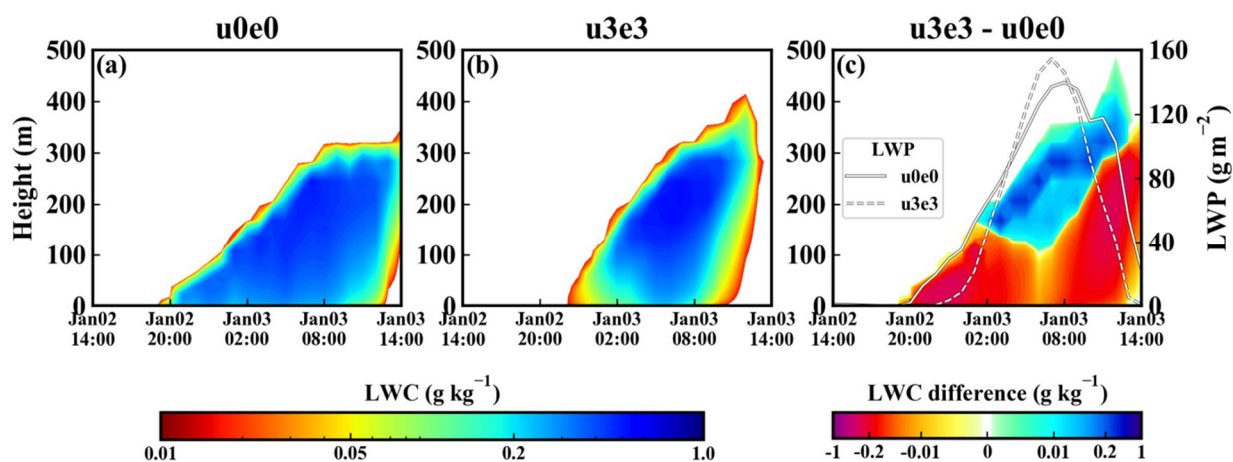
482

483 Figure 8. Relationships of the microphysical parameters (LWC, N<sub>d</sub>, R<sub>e</sub> and LWP) with emission level. These param-  
484 eters are the time-height averages (time average for the LWP), taking only non-zero values into consideration.

485



486



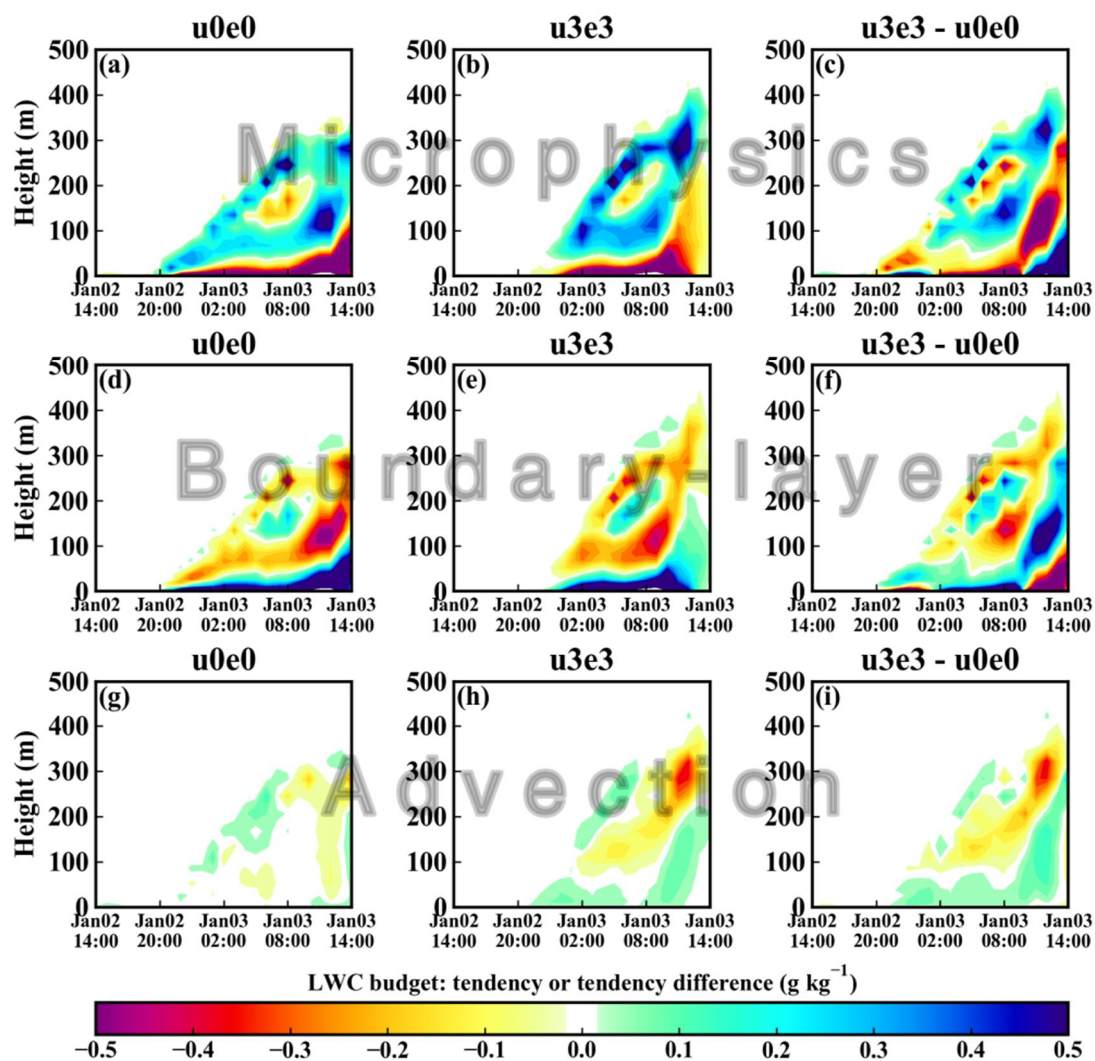
487

488 Figure 9. Similar to Fig. 5, but for the combined effect of urbanization and aerosols (u3e3 minus u0e0).

489



490

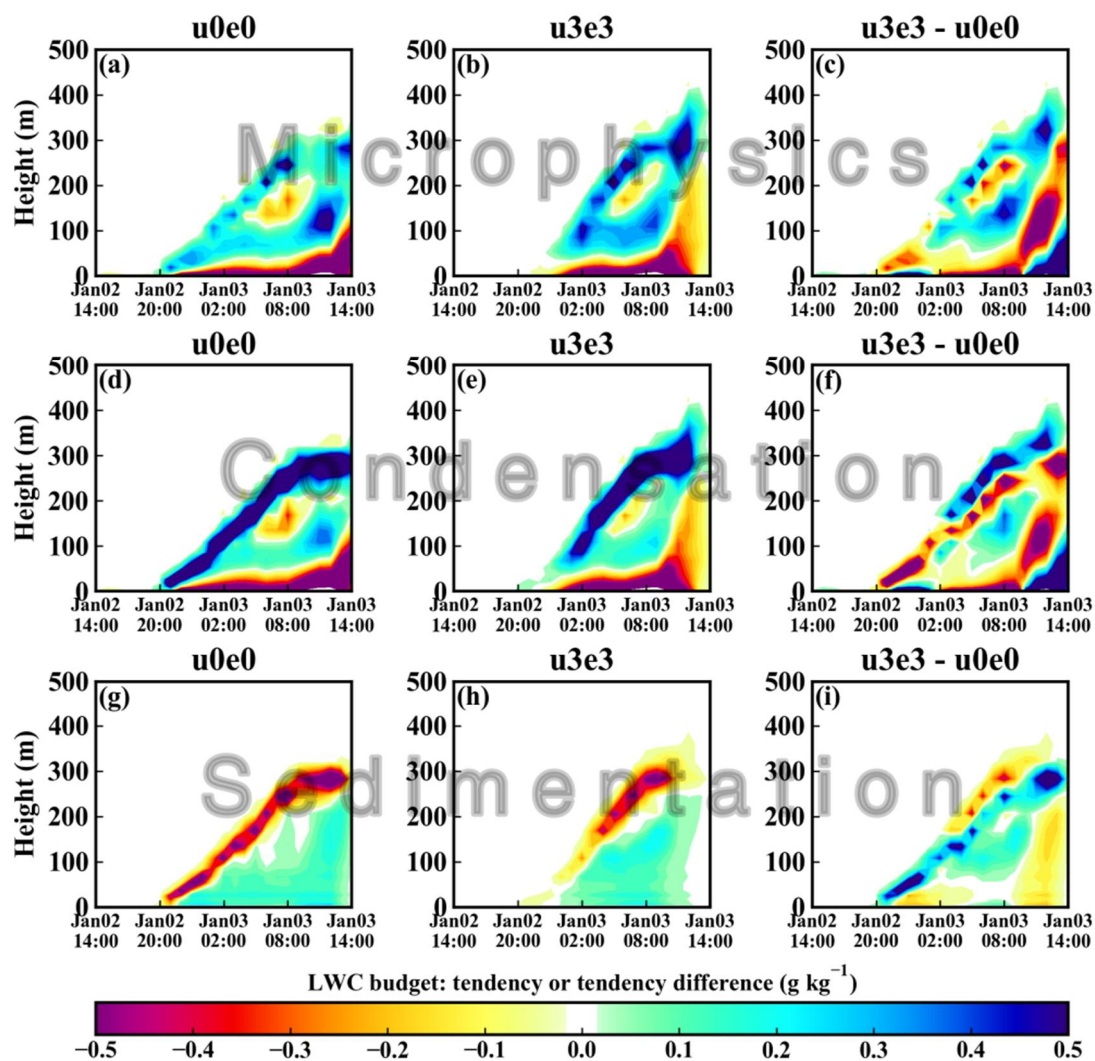


491

492 Figure 10. The combined effect of urbanization and aerosols (u3e3 minus u0e0) on various items of the LWC budget.  
493 The three rows are the 1-hour accumulated tendencies ( $\text{g kg}^{-1}$ ) of the microphysical, boundary layer, and advection  
494 processes.  
495



496



497

498 Figure 11. The combined effect of urbanization and aerosols (u3e3 minus u0e0) on various items of the microphysical  
499 tendency. The three rows are the 1-hour accumulated tendencies ( $\text{g kg}^{-1}$ ) of the microphysical, condensa-  
500 tion/evaporation, and sedimentation processes.

501